

Supplementary Information

Supramolecular Structures of Terbium (III) Porphyrin Double-Decker Complexes on Single-Walled Carbon Nanotube Surface

Ahmed I. A. Abd El-Mageed,* and Takuji Ogawa*

Abstract: This work mainly reports observation of novel supramolecular structures of Tb^{III}-5,15-bisdodecylporphyrin (BDP, C12P) double-decker complex on the surfaces of single-walled carbon nanotubes (SWNTs) performed by scanning tunneling microscopy under an ultra-high vacuum and low temperature, atomic force microscopy, scanning electron microscopy coupled with energy dispersive spectroscopy, and ultraviolet–visible spectroscopy. The molecules formed a well-ordered self-assembled helix-shaped array with regular periodicity on the tube surface. Additionally, some magnetic properties of the BDP–molecule as well as the resulting BDP–SWNT composites were investigated by superconducting quantum interference measurements. The molecule exhibits single-molecule magnetic (SMM) properties and the composite’s magnetization increases almost linearly with decreasing temperature which possibly due to the coupling between porphyrin molecules and SWNT. Consequently, this may enable the development of more advanced spintronic devices based on porphyrin–nanocarbon composites.

Author Contributions

Ahmed. I. A. A. suggested the proposal, performed the SPM measurements, molecular synthesis, and fabricated the complexes, carried out spectroscopic and SEM-EDS measurements, calibrated STM images as well as DFT calculations. T. O. guided the research and supervised all the studies. Ahmed. I. A. A. wrote the manuscript. The authors discussed the results and commented on it.

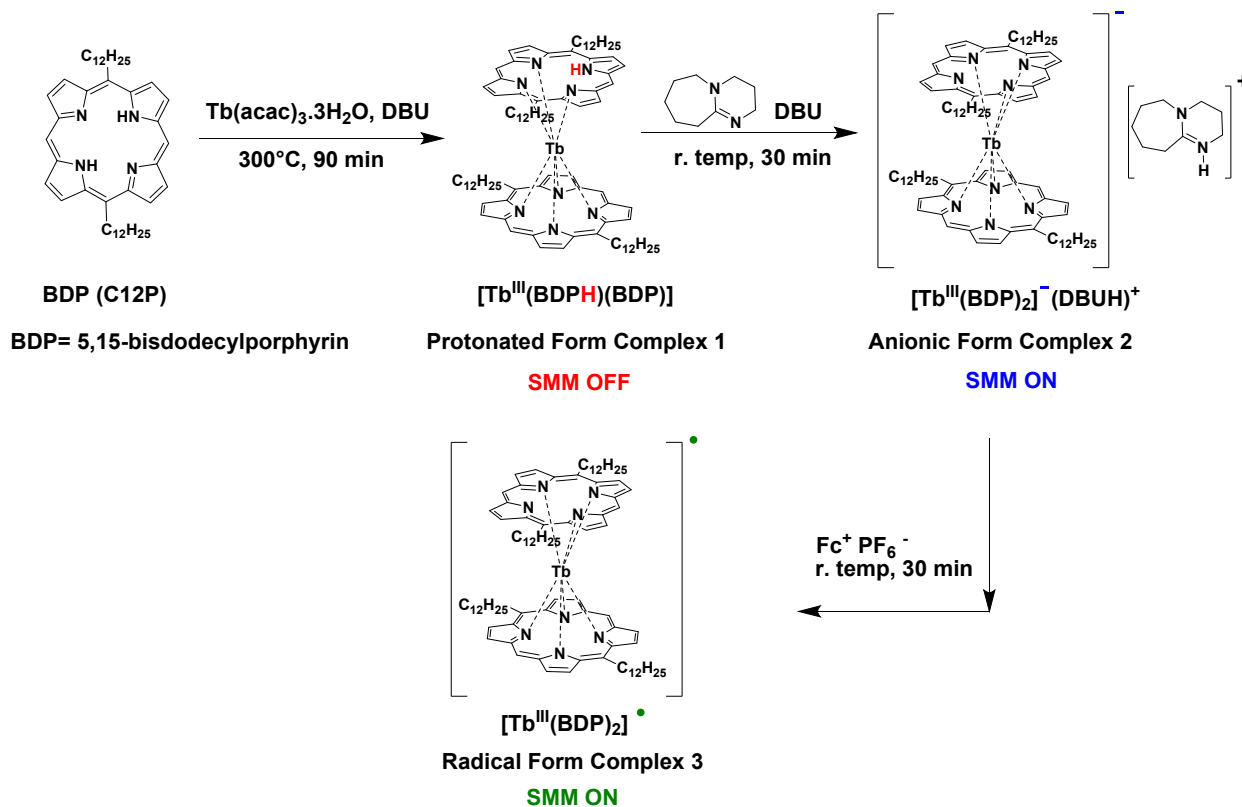
Table of Contents

Synthesis and Characterization	S3
Characterization Techniques	S3
Purification of Raw-HiPCO SWNT	S4
UV-Vis of Raw-HiPCO SWNT	S4
DFT Calculations and Molecular Modeling	S4
UV-Vis Spectra of Tb-Porphyrin Double-Decker Complexes	S5
Supramolecular Structures of Tb-Porphyrin Double-Decker Complexes on SWNT Surface observed by Ultra-High Vacuum Scanning Tunneling Microscopy (UHV-STM) at Low Temperatures	S6
Supramolecular Structures of Tb-Porphyrin Double-Decker Complexes on SWNT Surface observed by Atomic Force Microscopy (AFM) under Ambient Conditions	S7
Magnetic Measurements of protonated form 1, anionic form 2 and radical form 3 Complexes	S8
Magnetic Measurements of 2-SWNT and 3-SWNT composites	S9
Magnetic Measurement of 1-SWNT composite	S10
Magnetic Measurements of Purified-HiPCO SWNT	S10
SEM coupled EDS measurements of Purified-HiPCO SWNT	S12

Experimental Section

Synthesis and Characterization

The target complexes i.e. protonated **1**, anionic **2** as well as radical **3** forms have been synthesized as depicted in Scheme S1.



Scheme S1. Procedures for synthesizing protonated form **1**, anionic form **2** and radical form **3** complexes of Tb^{III}-5,15-bisdodecylporphyrin.

Characterization Techniques

Mass spectra were recorded using a Shimadzu AXIMA-CFR MALDI-TOF mass spectrometer. UV-Visible adsorption spectra were carried out on a Shimadzu UV-3150 double-beam spectrophotometer. The SEM-EDS image was captured on a JEOL JSM-7600F microscope equipped with an EDS analyzer. The applicable range of acceleration voltage at normal measurement: 1–30 kV with maximum resolution of about 1 nm. Elemental analysis was performed by using a Yanaco CHN CORDER MT-5 instrument. Atomic force microscopic measurements were recorded using JEOL SPM-5200 scanning probe microscope (SPM). All the AFM images were taken using tapping mode under ambient conditions on HOPG surface.

The STM measurements were conducted using OMICRON scanning probe microscope with NanoNis software, Germany. All STM images were captured in a constant current mode under ultra-high vacuum and low temperature. The STM tip has been purchased from the provider, where it is prepared using special preparation tool, and have been used as received. The tip preparation tool is designed for efficient cleaning of SPM tunneling tips from etching remains or oxides which can create artefacts or unstable tips during imaging or spectroscopy applications. This process requires temperatures above 1000 °C at the tip to remove those remains. From a thoriated tungsten filament in the tip preparation tool electrons are emitted. Due to the electron bombardment the SPM tip is cleaned from deposits.

Magnetic susceptibility measurements were performed using a Quantum Design MPMS-XL AC (Super-Conducting Quantum Interference Device, SQUID) magnetometer. Alternating current (ac) measurements were performed at various frequencies from 1 to 997 Hz with an ac field amplitude of 3.9 G in the presence of a direct current (dc) field (zero and 2000 Oe), however the direct current (dc) measurements were conducted at 2000 Oe field under different temperature range from 2 to 300 K. Measurements were carried out on a randomly oriented powder sample with magnetic field.

Purification of Raw-HiPCO SWNT

Since we used raw HiPCO-SWNTs, the sample was purified from amorphous carbon and metal catalysts by heating and refluxing with concentrated mineral acids i.e. HCl, respectively. The sample was then washed with an aqueous solution of NaHCO₃ to be neutralized. Thereafter, SWNT was dried in the oven for further usage. The detailed purification steps have been reported in our previous study.¹

UV-Vis of Raw-HiPCO SWNT

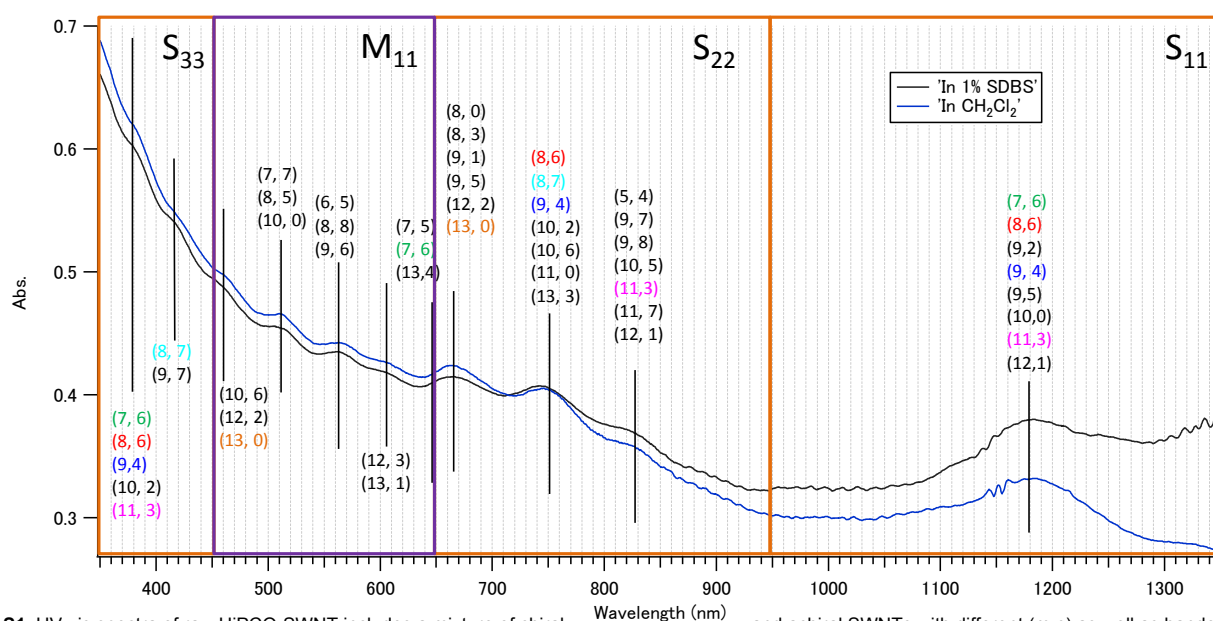


Figure S1. UV-vis spectra of raw HiPCO-SWNT includes a mixture of chiral and achiral SWNTs with different (m,n) as well as handedness chiralities, dispersed in both CH₂Cl₂ and sodium dodecyl benzene sulfonate (SDBS).

Results and Discussion

DFT Calculations and Molecular Modeling

The optimized structure of the [Y(BDP)₂]⁺ calculated using density functional theory (DFT) calculation with B3LYP/3-21G (for C, H, N) & SDD (for Y) functional level as well as the frontier molecular orbitals (HOMO and LUMO) and their absolute energies values are demonstrated in Figure S2 and Table S1, respectively.

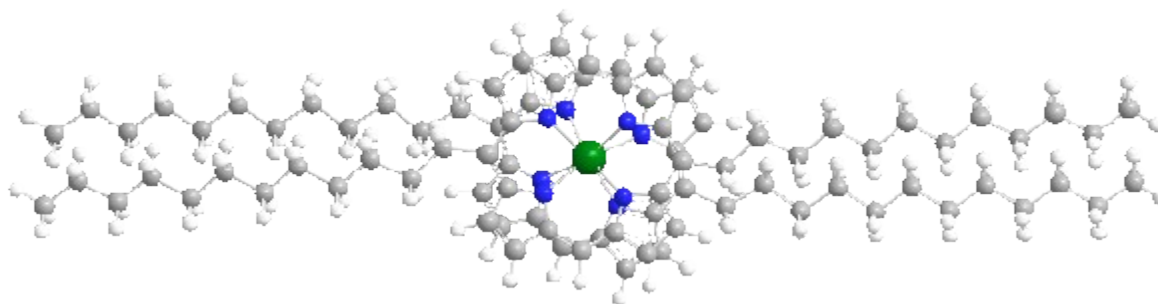


Figure S2. Optimized geometric structure of [Y(BDP)₂]⁺ calculated using DFT calculation with B3LYP/3-21G (for C, H, N) & SDD (for Y) functional level. In the modeling, C-atoms are shown with the grey color, H in white, iridium Y in green and N in blue.

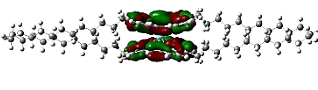

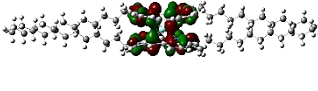
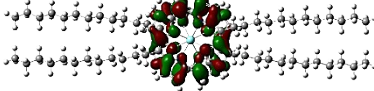
	Side View	Top View
$[Y(BDP)_2]^-$ α -HOMO	 - 4.379 eV	 - 4.379 eV
$[Y(BDP)_2]^-$ α -LUMO	 - 2.168 eV	 - 2.168 eV

Table S1. The frontier molecular orbitals (HOMO and LUMO) and their absolute energies values of $[Y(BDP)_2]^-$ (α -shape) calculated using DFT calculation with B3LYP/3-21G (for C, H, N) & SDD (for Y) functional level.

UV-Vis Spectra of Tb-Porphyrin Double-Decker Complexes

The Soret peaks of the protonated form **1** (392 nm) and anionic form **2** (396 nm) were blue-shifted relative to that of the BDP (C12P) ligand (404 nm); however, this peak was red-shifted for the anionic form **2** relative to the protonated form **1** (Figure S3). According to the literature²⁻⁴ the radical forms of porphyrin and phthalocyanine double-decker complexes have a characteristic broad Q-band in the near-infrared (NIR) region together with the Soret band (UV-vis region). Therefore, an NIR absorption band was observed at 1153 nm, in addition to the blue shift of the Soret peak of the radical form **3** (387 nm) relative to those of the BDP ligand (404 nm), protonated form **1** (392 nm), and anionic form **2** (396 nm). In the radical form **3**, the cofacial distance between the two porphyrin rings decreases because of an increase in the bond order, due to the removal of an electron from the antibonding orbital of the HOMO,⁵⁻⁹ ultimately resulting in blue-shifting of the Soret band of **3** (Figure S3).

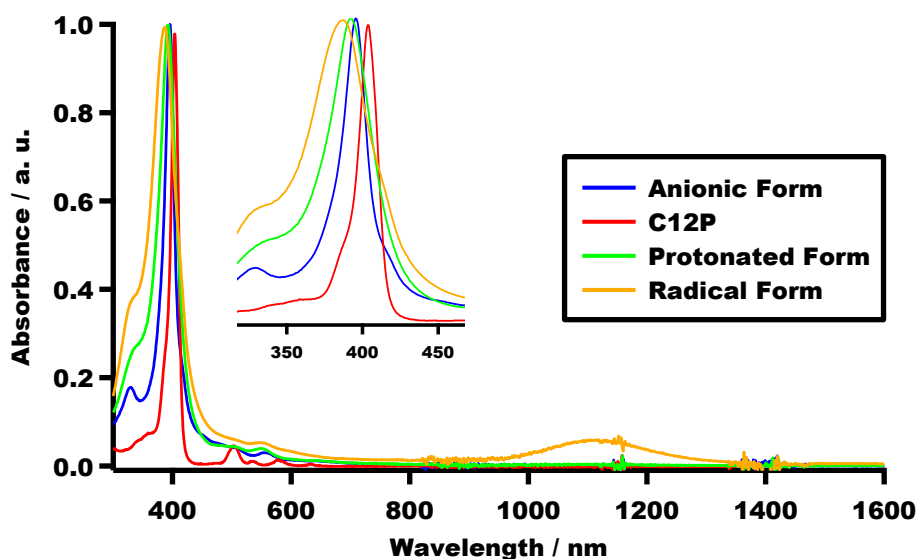


Figure S3. UV-Vis spectra of BDP (C12P), protonated **1**, anionic **2**, and radical **3** form complexes in dichloromethane.

Supramolecular Structures of Tb-Porphyrin Double-Decker Complexes on SWNT Surface observed by Ultra-High Vacuum Scanning Tunneling Microscopy (UHV-STM) at Low Temperatures

The STM measurements were conducted using OMICRON scanning probe microscope with NanoNis software, Germany. All STM images were captured in a constant current mode under ultra-high vacuum and low temperature. The supramolecular structures of BDP-SWNT composite samples on HOPG surface were prepared using simple drop casting technique (i.e. drops of the dispersed composites in MeOH (ca. 5 μ l) were casted onto a freshly cleaved HOPG surfaces) and fixed onto the cell. The sample was then left to dry at room temperature to be ready for observation. All the images were captured under ultra-high vacuum and low temperature (i.e. 80 K). To induce a tunneling current, a bias voltage was applied between sample and the tip. Image calibration was done using Gwyddion software.

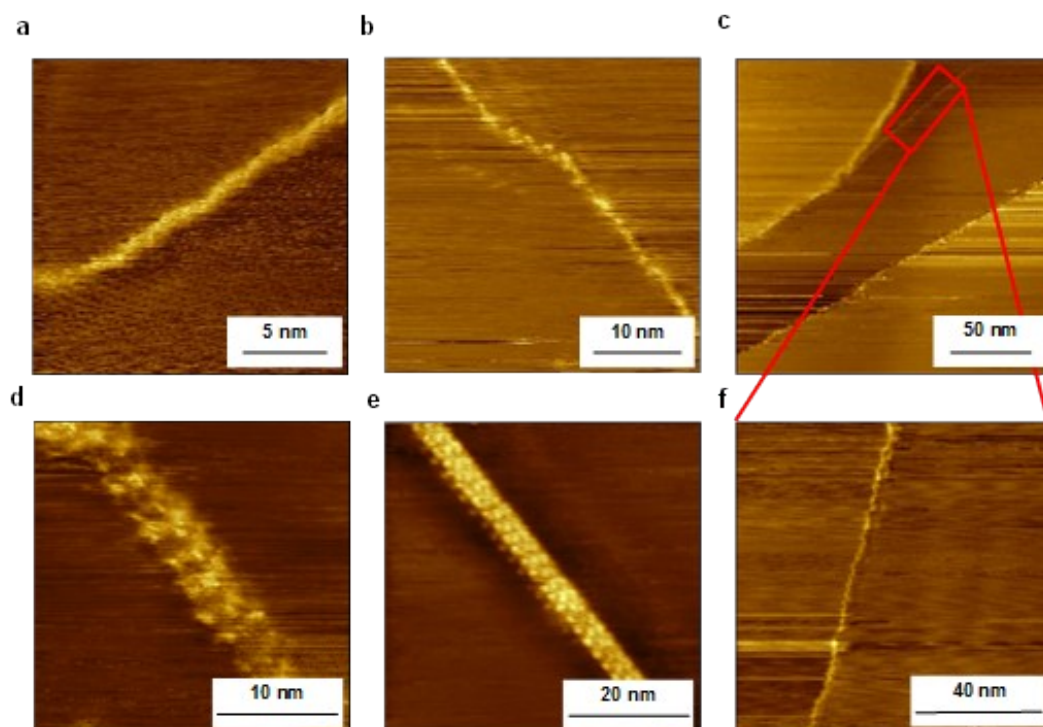


Figure S4. Typical STM images for supramolecular structures of 3-SWNT composite on HOPG surface. **a**, 3-SWNT composite ($I_t = 0.1$ nA, $V_{\text{sample}} = 0.7$ V). **b**, 3-SWNT composite ($I_t = 0.05$ nA, $V_{\text{sample}} = 0.5$ V). **c**, 3-SWNT composite ($I_t = 0.1$ nA, $V_{\text{sample}} = 0.7$ V). **d**, 3-SWNT composite ($I_t = 0.05$ nA, $V_{\text{sample}} = 0.1$ V). **e**, 3-SWNT composite ($I_t = 0.05$ nA, $V_{\text{sample}} = 0.08$ V). **f**, 3-SWNT composite ($I_t = 0.1$ nA, $V_{\text{sample}} = 0.5$ V).

Supramolecular Structures of Tb-Porphyrin Double-Decker Complexes on SWNT Surface observed by Atomic Force Microscopy (AFM) under Ambient Conditions

AFM is used as an effective tool to investigate the supramolecular structures of **3** on SWNT surface, by casting a few drops of the dispersed composite in MeOH on a freshly cleaved HOPG surface.

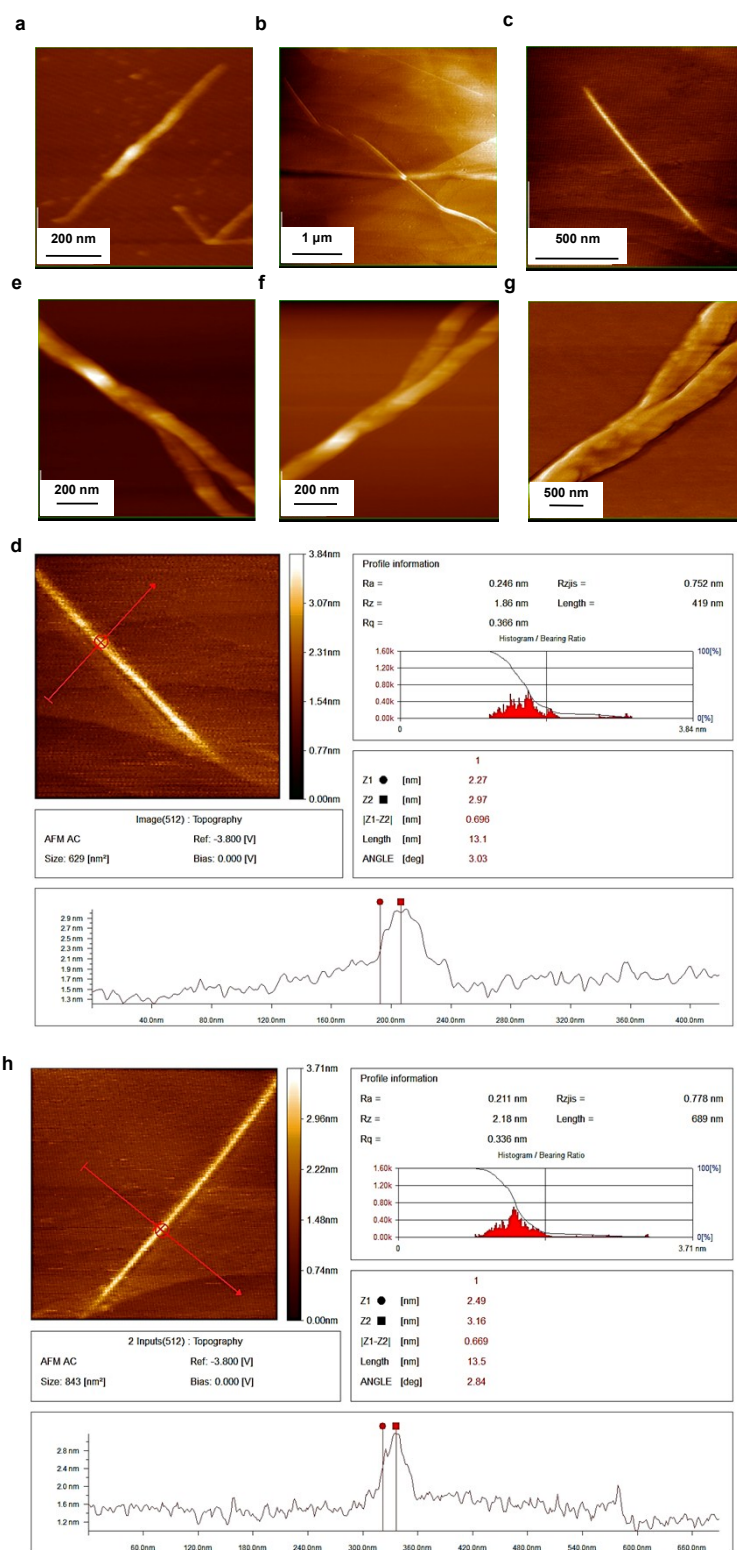


Figure S5. (a-c; e-g). Typical AFM images (topographic and phase) for supramolecular structures of **3**-SWNT composite on HOPG surface under ambient conditions. **d, h** The topographic profiles for **3**-SWNT composite, represent the average molecular height around 0.677 nm.

Magnetic Measurements of protonated form 1, anionic form 2 and radical form 3 Complexes

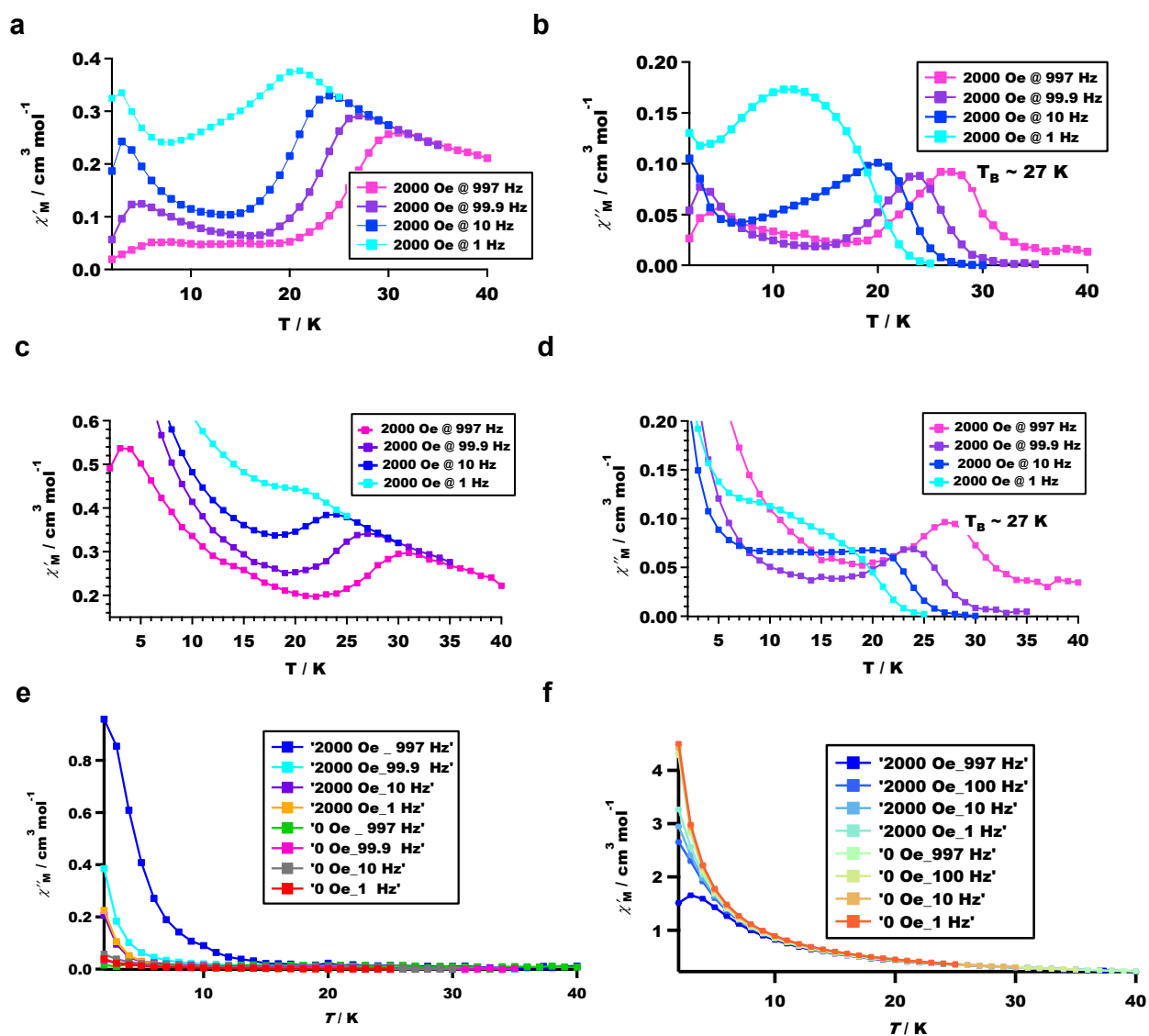


Figure S6. Temperature dependence of in-phase (χ'_M) and out-of-phase (χ''_M) ac magnetic susceptibility of anionic form 2 (a, b), radical form 3 (c, d), under 2000 Oe dc magnetic field. (e, f), Temperature dependence of in-phase (χ'_M) and out-of-phase (χ''_M) ac magnetic susceptibility of protonated form 1 under zero and 2000 Oe dc magnetic fields shows that protonated form 1 doesn't act as SMM.

Magnetic Measurements of 2-SWNT and 3-SWNT composites

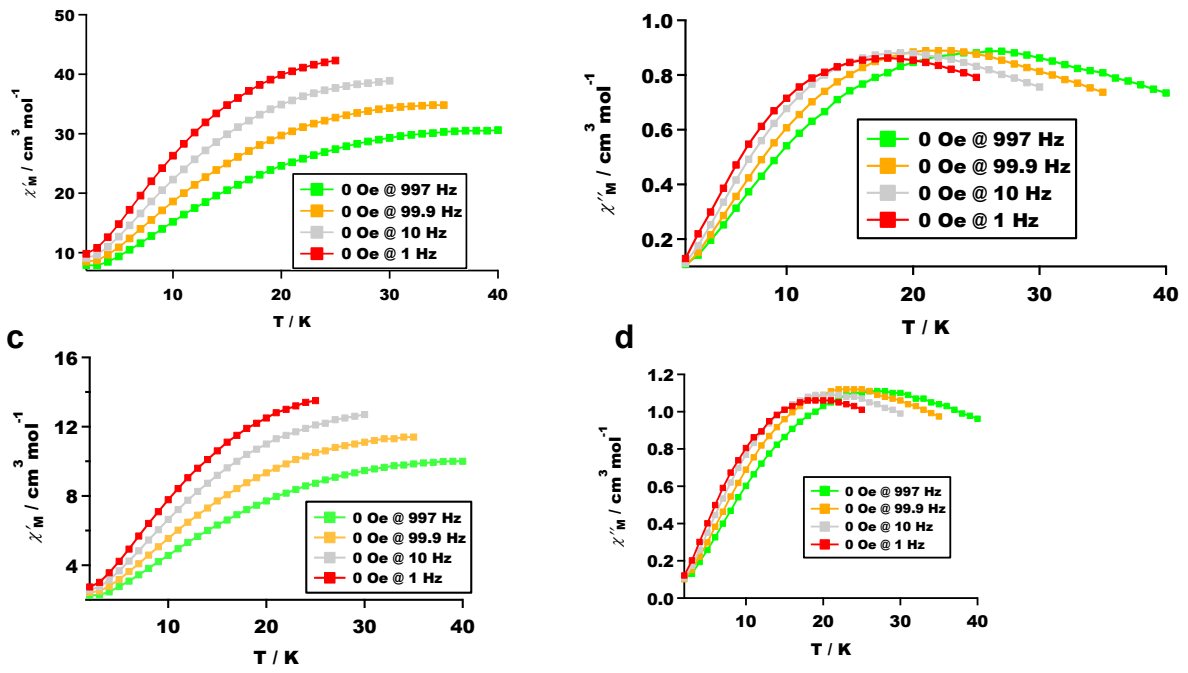


Figure S7. Temperature dependence of in-phase (χ'_M) and out-of-phase (χ''_M) ac magnetic susceptibility of 2-SWNT composite (a, b), 3-SWNT composite (c, d), under 0 Oe dc magnetic field.

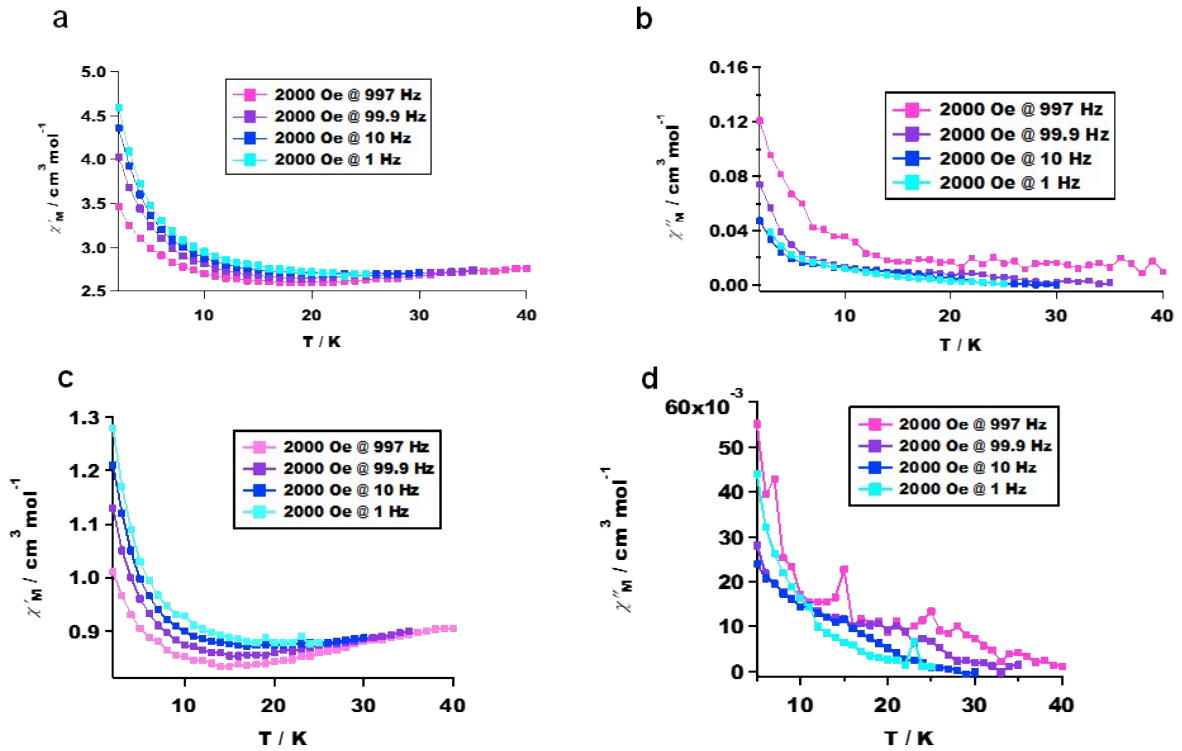


Figure S8. Temperature dependence of in-phase (χ'_M) and out-of-phase (χ''_M) ac magnetic susceptibility of 2-SWNT composite (a, b), 3-SWNT composite (c, d), under 2000 Oe dc magnetic field.

Magnetic Measurement of 1-SWNT composite

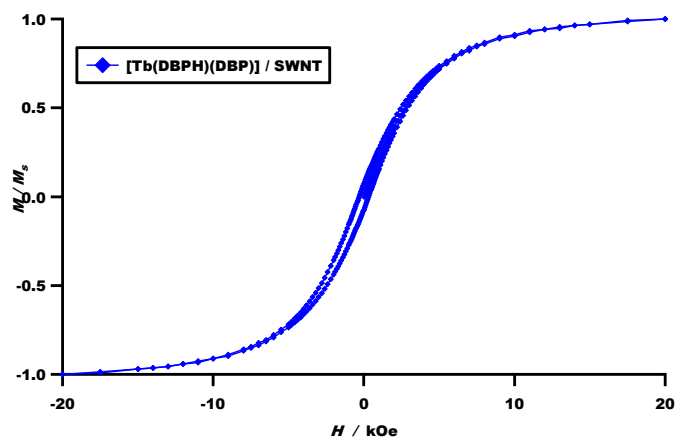


Figure S9. Hysteresis loop of the 1-SWNT composite at 1.8 K within ± 20 kOe.

Magnetic Measurements of Purified-HiPCO SWNT

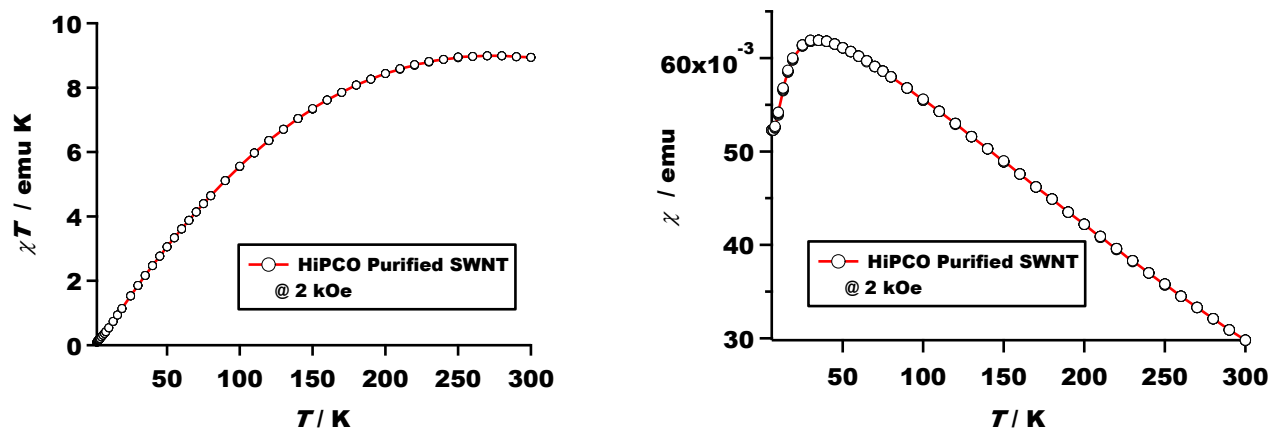


Figure S10. Temperature dependence of the dc magnetic susceptibility measurements of purified-HiPCO SWNTs under a constant magnetic field of 2 kOe.

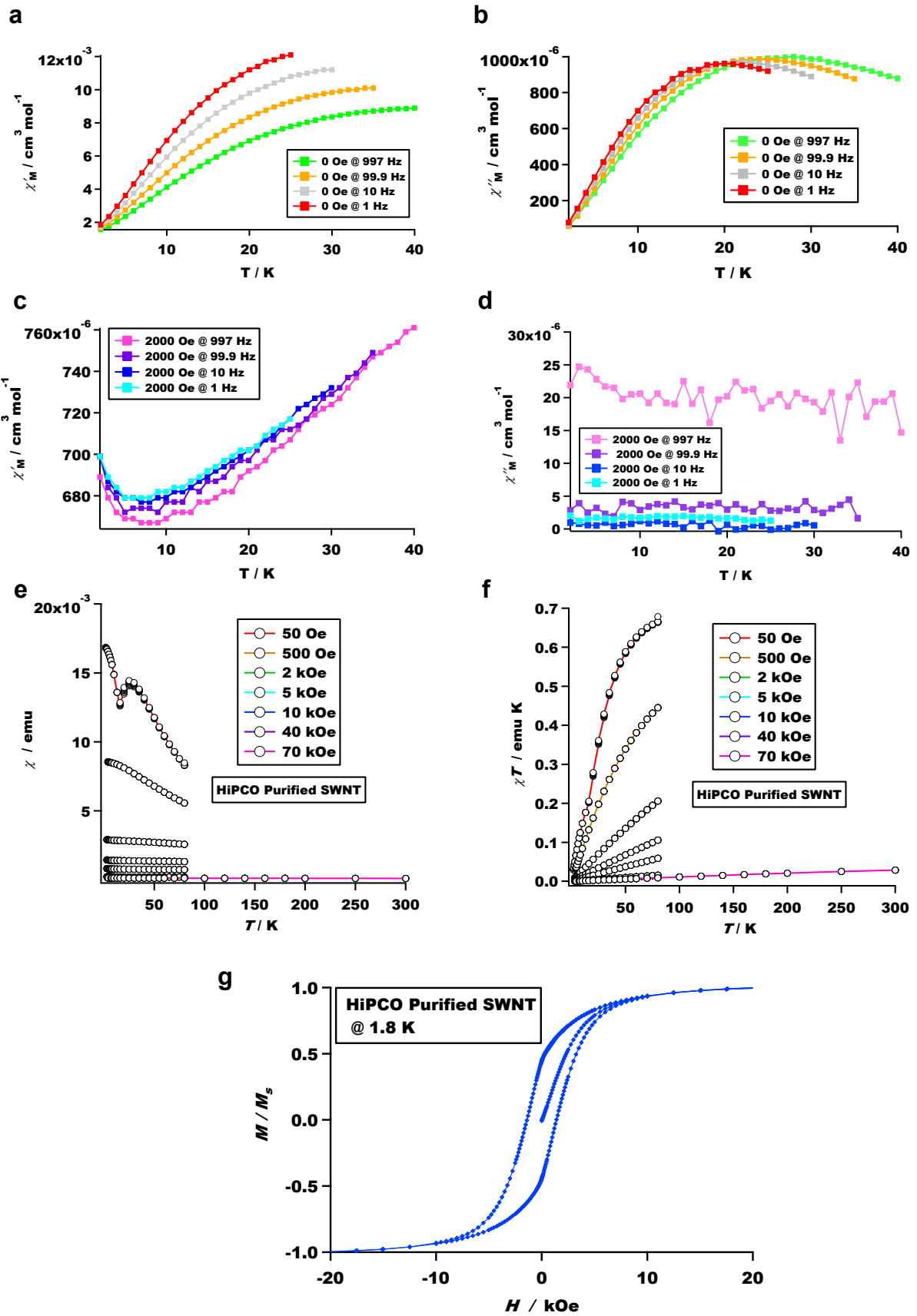


Figure S11. Temperature dependence of in-phase (χ'_M) (a, c) and out-of-phase (χ''_M) (b, d) ac magnetic susceptibility of purified-HiPCO SWNT, under zero and 2000 Oe dc magnetic field. (e) Temperature dependence of the magnetic susceptibility of purified-HiPCO SWNT at different applied magnetic field between 50 Oe and 4 T for temperatures below 100 K, and up to 7 T at 300 K. (f) Field dependence of the magnetization of purified-HiPCO SWNT (from 50 Oe to 4 T) for temperatures below 100 K, and up to 7 T at 300 K. (g) Hysteresis loop of the purified-HiPCO SWNT at 1.8 K within ± 20 kOe.

SEM coupled EDS measurements of Purified-HiPCO SWNT

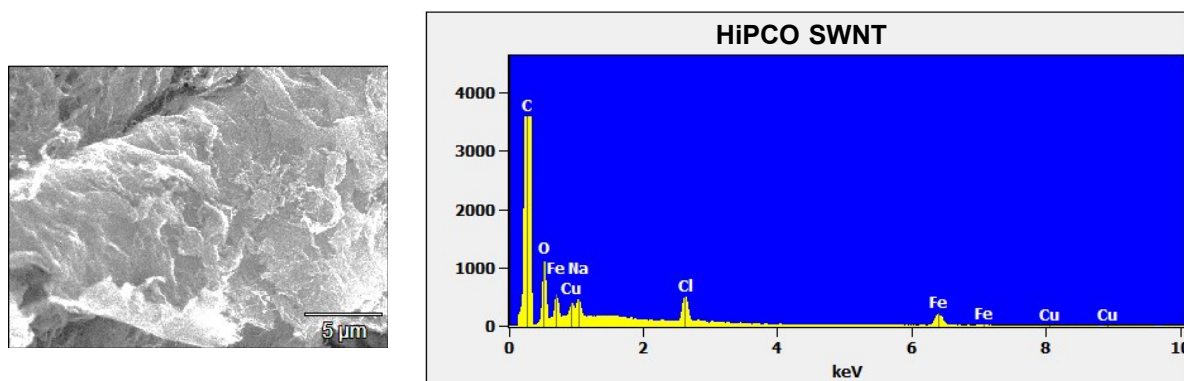


Figure S12. SEM coupled EDS measurement of purified-HiPCO SWNT.

References

1. A. I. A. El-Mageed and T. Ogawa, *Appl. Surf. Sci.*, 2018, **462**, 904-912.
2. M. Damjanović, Y. Horie, T. Morita, Y. Horii, K. Katoh, M. Yamashita and M. Enders, *Inorg. Chem.*, 2015, **54**, 11986-11992.
3. Y. Chen, F. Ma, X. Chen, B. Dong, K. Wang, S. Jiang, C. Wang, X. Chen, D. Qi and H. Sun, *Inorg. Chem. Front.*, 2017, **4**, 1465-1471.
4. J. Buchler, P. Hammerschmitt, I. Kaufeld and J. R. Loffer, *Chem. Ber.*, 1991, **124**, 2151-2159.
5. R. J. Donohoe, J. K. Duchowski and D. F. Bocian, *J. Am. Chem. Soc.*, 1988, **110**, 6119-6124.
6. J. W. Buchler and B. Scharbert, *J. Am. Chem. Soc.*, 1988, **110**, 4272-4276.
7. J. W. Buchler, J. Hüttermann and J. Löffler, *Bull. Chem. Soc. Jpn.*, 1988, **61**, 71-77.
8. J. K. Duchowski and D. F. Bocian, *J. Am. Chem. Soc.*, 1990, **112**, 3312-3318.
9. G. A. Spyroulias, C. P. Raptopoulou, D. de Montauzon, A. Mari, R. Poilblanc, A. Terzis and A. G. Coutsolelos, *Inorg. Chem.*, 1999, **38**, 1683-1696.